7-6-2006

Oxygen Production and Carbon Sequestration in an Upwelling Coastal Margin

B. Hales

Lee Karp-Boss
University of Maine - Main, lee.karp-boss@maine.edu

A. Perlin

P. A. Wheeler

Oxygen production and carbon sequestration in an upwelling coastal margin

Burke Hales,[1] Lee Karp-Boss,[2] Alexander Perlin,[1] and Patricia A. Wheeler[1]

Received 25 March 2005; revised 7 December 2005; accepted 13 February 2006; published 6 July 2006.

[1] We examined high-resolution cross-shelf distributions of particulate organic carbon (POC) and dissolved O_2 during the upwelling season off the Oregon coast. Oxygen concentrations were supersaturated in surface waters, and hypoxic in near-bottom waters, with greatly expanded hypoxic conditions late in the season. Simplified time-dependent mass balances on cross-shelf integrated concentrations of these two parameters, found the following: (1) The average net rate of photosynthesis generated 2.1 mmol O_2 m^{-3} d^{-1} and (2) essentially none of the corresponding net carbon fixation of 1.4 mmol m^{-3} d^{-1} could be accounted for in the observed standing stocks of POC. After examining other possible sinks for carbon, we conclude that most of the net production is being exported to the adjacent deep ocean. A simplified POC budget suggests that about a quarter of the export is via alongshore advection, and the remainder is due to some other process. We propose a simplistic conceptual model of across-shelf transport in which POC sinks to the bottom boundary layer where it comes into contact with mineral ballast material but is kept in suspension by high turbulence. When upwelling conditions ease, the BBL waters move seaward, carrying the suspended, ballasted POC with it where it sinks rapidly into the deep ocean at the shelf break. This suggests a mechanism whereby the duration and frequency of upwelling events and relaxations can determine the extent to which new carbon produced by photosynthesis in the coastal ocean is exported to depth rather than being respired on the shelf.

Citation: Hales, B., L. Karp-Boss, A. Perlin, and P. A. Wheeler (2006), Oxygen production and carbon sequestration in an upwelling coastal margin, *Global Biogeochem. Cycles*, *20*, GB3001, doi:10.1029/2005GB002517.

1. Introduction

[2] Coastal upwelling areas experience intense biological productivity in response to the nutrient supply. Although such areas occupy roughly 1% of the total ocean surface area, they account for over 10% of the global new productivity [*Chavez and Toggweiler*, 1995]. Satellite-based estimates suggest that as much as 40% of the global ocean's export productivity occurs in the coastal oceans [*Muller-Karger et al.*, 2005]. The significance of coastal oceans in global exchange of CO_2 with the atmosphere is now receiving significant attention[(e.g., *Bianchi et al.*, 2005; *Cai et al.*, 2003; *Chen et al.*, 2004; *Hales et al.*, 2005a; *Thomas et al.*, 2004]. Coastal regions are vulnerable to eutrophication and hypoxia [*Richardson and Jorgensen*, 1996], often due to terrestrial or anthropogenic nutrient loading, but the impact of exchange of coastal and open ocean waters is now being recognized as another driver for coastal hypoxia [*Grantham et al.*, 2004; *Glenn et al.*, 2004].

[3] The Oregon coastal ocean is a region of intense seasonal upwelling: Prevailing summer winds blow alongshore, creating offshore Ekman transport in surface waters, which in turn draws dense, nutrient-rich offshore water up and shoreward [e.g., see *Barth and Wheeler*, 2005]. Nitrate from this upwelled water is then mixed upward into the euphotic zone [*Hales et al.*, 2005b]. Corresponding to this upwelling and upward turbulent transport is a massive photosynthetic response by a diatom-dominated phytoplankton community, with standing stocks of chlorophyll and particulate organic carbon (POC) reaching concentrations in excess of 20 μg kg^{-1} and 100 μmol kg^{-1}, respectively [*Barth and Wheeler*, 2005; *Castelao and Barth*, 2005; *Eisner and Cowles*, 2005; *Ruttenberg and Dhyrmann*, 2005; *Karp-Boss et al.*, 2004; *Hill and Wheeler*, 2001; *Neuer and Cowles*, 1994; *Small et al.*, 1989]. This has been shown to drive Oregon coastal surface water CO_2 levels far below atmospheric saturation [*Hales et al.*, 2005a]. The POC can subsequently rain from the surface into already low-O_2 upwelled source waters near the bottom. If it is respired there, further O_2 depletion can result, leading to hypoxic conditions. Recently documented severe hypoxia in near-bottom waters off the Oregon coast has led to fish and crab kills there [*Grantham et al.*, 2004; *Service*, 2004].

[4] The former observation leads to the question of the fate of the CO_2 taken up from the atmosphere. If POC is

[1]College of Oceanic and Atmospheric Sciences, Oregon State University, Corvallis, Oregon, USA.
[2]School of Marine Sciences, University of Maine, Orono, Maine, USA

0886-6236/06/2005GB002517

quantitatively respired over the course of the season, CO_2 may be released to the atmosphere following transition to the typical stormy winter downwelling conditions [*Barth and Wheeler*, 2005], and the summertime CO_2 uptake is largely canceled out on seasonal timescales. If, however, the fixed POC is transported to the shelf break and subsequently sinks to depths below that of the seasonally upwelled source waters [e.g., *Walsh*, 1991; *Walsh et al.*, 1991, 1988], it will be lost from the surface-ocean atmosphere system on timescales corresponding to the age of the permanent thermocline of the North Pacific: decades to centuries.

[5] The latter observation has been attributed to changes in the O_2 content of the upwelled source water [*Grantham et al.*, 2004], possibly driven by shifts in long-term climate-forcing parameters such as the Pacific Decadal Oscillation (PDO) (see, e.g., summary by *Huyer* [2003]). However, the O_2 content of deep upwelled waters that actually cover most of the shelf seafloor was at or below hypoxic thresholds in 2001 (presented here). Yet in 2001 no evidence of hypoxia's effects on fish or invertebrates was reported, while in 2002 these reports were extensive. These results prompt the question of what can drive the difference in conditions between the two years.

[6] Both of the above are centrally dependent on resolving the relative contributions of local respiration of shelf POC and its off-shelf transport. In the following sections we present observations of high spatial-resolution cross-shelf and vertical distributions of dissolved O_2 and POC spanning the upwelling season in 2001. We perform time-dependent mass balance calculations to constrain the average net O_2 productivity, and compare this to the changes in POC standing stock over the same time interval. These procedures directly address the above questions. This work was undertaken as part of the Coastal Ocean Advances in Shelf Transport (COAST; http://damp.oce.orst.edu/coast) project, sponsored by the National Science Foundation's Coastal Ocean Processes program (http://www.skio.peachnet.edu/research/coop/), in which the authors participated.

2. Experimental Setting and Methods

[7] The field study took place during May and August of 2001 aboard the R/V *Thomas G. Thompson*. A series of cross-shelf transects which were executed at several locations between Cascade Head, at 45°00'N, and Cape Perpetua, on the south flank of Heceta Bank, at 44°22′N (Figure 1a). Complete sections at Cape Perpetua were occupied once in May and August, while the Cascade Head section was occupied repeatedly in May, and once in August. While the data collected on sections between these two locations are consistent with the observations at the northern and southern extremes, they did not reliably span the distance between the shoreline and the shelf break in May and August, and so are not used to constrain flux balances here. As the shelf is narrow at Cascade Head and broad at Cape Perpetua, the cross-shelf areas of the two sections are quite different ($\sim$2.4 km^2, and 5.9 km^2, respectively). Wind records for the entire summer and the two cruises (Figures 1b–1d) show the expected pattern of predominantly equatorward, upwelling favorable winds, with brief periods of relaxations of winds speeds and/or reversals in wind direction. Winds are generally coherent throughout the region, [*Perlin et al.*, 2004] with good agreement between buoy-based (Figure 1b) and ship-based (Figures 1c–1d) wind records. Wind forcing throughout the season (Figure 1b) was similar to that during the two cruises. This combined with the observation that remotely sensed SST and ocean color was similar throughout the season (R. Letelier, personal communication, 2005) suggests that the conditions during the two cruises were representative of the entire upwelling season.

[8] High-resolution distributions of O_2 concentration, density, and optical beam attenuation (beam-C) were measured using a system developed by Hales and colleagues at OSU (hereafter SuperSucker). SuperSucker was precisely positioned on a target depth versus time curve, using remote autonomous winch control, while towed by the ship. In situ instrumentation aboard SuperSucker included a SeaBird 9+ CTD unit, interfaced with sensors for measurement of pressure (and hence depth), altitude (which allowed the system to sample the bottom boundary layer and avoid hitting the seafloor), temperature and conductivity (which allow calculation of salinity, and density, presented hereafter as σ_t) in addition to those for O_2 and beam-C. SuperSucker followed a target curve that was defined by a prescribed ascent and descent rate of 0.3 m s^{-1}, and deep and shallow limits of 2 m above the bottom and below the sea surface, respectively. The sampling path was an expanding sawtooth whose horizontal resolution grew from <200 m at the shallow, inshore ends of the transects to about 1 km at the deep, shelf-break ends. Vertical resolution of in situ measurements was 0.3 m, determined by SuperSucker's profiling speed and the reduction of the CTD data to 1-Hz frequency.

[9] SuperSucker carried a pump which delivered a constant 8 L min^{-1} seawater flow to the shipboard laboratory via a tube embedded in the tow cable and a rotating fluid joint in the winch's slip ring. Most important for this paper was the ability to regularly collect discrete samples at the shipboard end of the sampling line which ensured the accuracy of the electrode-based O_2 measurements, and defined the relationship between the beam-C and POC (Figures 2a and 2b).

[10] Oxygen concentrations were determined using a SeaBird SBE 23 electrode, whose raw output was converted to O_2 concentration (mL L^{-1}) using factory-supplied calibration algorithms and constants. These data were further calibrated and converted to units of μmol kg^{-1} against discrete samples collected from the shipboard end of the sample stream and analyzed by standard Winkler titration methods (Figure 2a). This calibration was highly linear over the range of concentrations observed, and was the same for the two cruises. Oxygen saturation concentrations (μmol kg^{-1}) were calculated in surface waters for in situ T and S using the algorithm of *Garcia and Gordon* [1992].

[11] Beam-C was measured using a WetLabs C-Star transmissometer (660 nm, 25-cm path length), whose raw output was converted to beam-C coefficients (m^{-1}) using factory supplied algorithms and reference values. To assure stability of the instrument's reading during the cruise, dark and DIW measurements were taken, and the instrument's

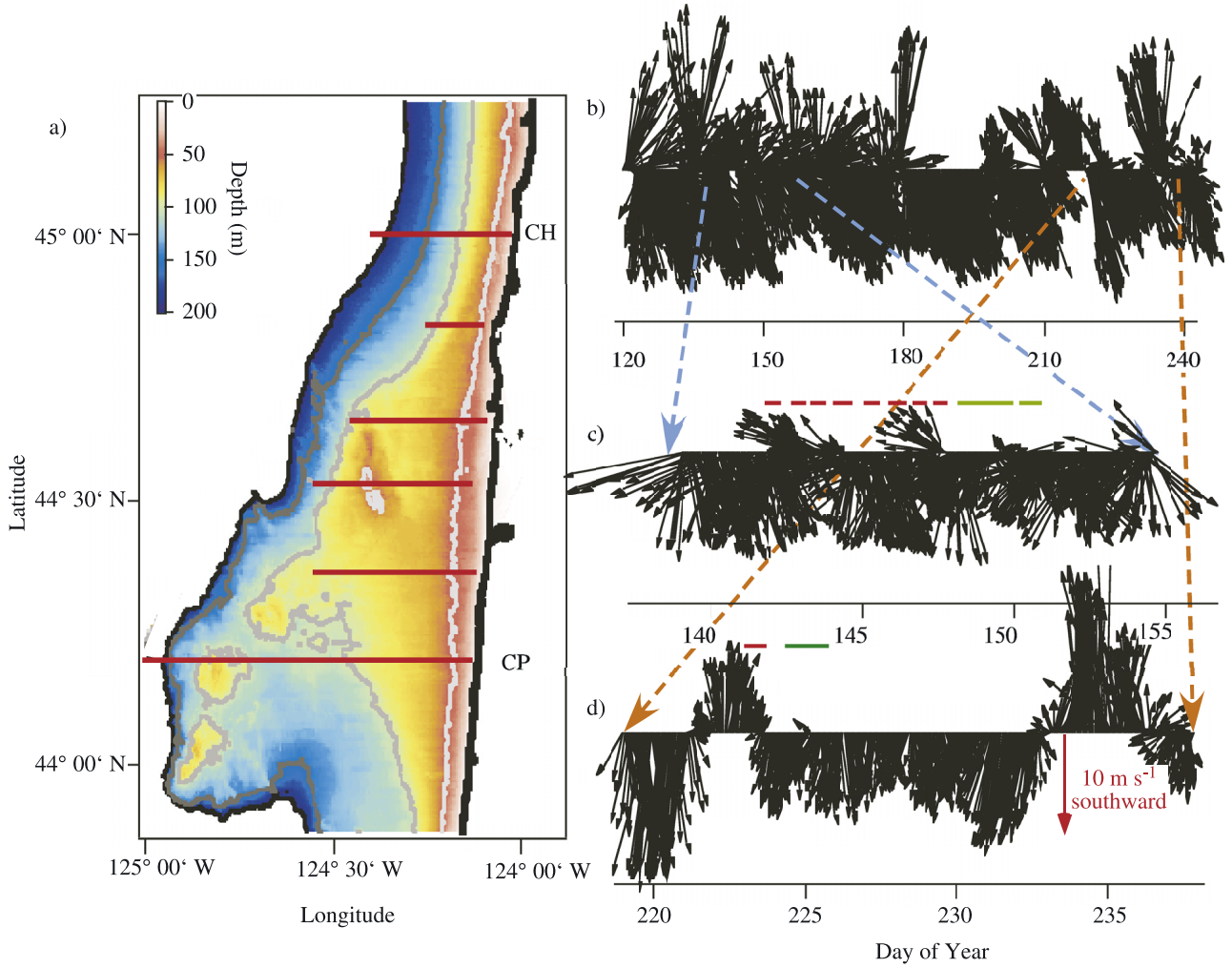

Figure 1. (a) Map of the study area, showing the locations of the Cascade Head (CH) and Cape Perpetua (CP) sections at the northern and southern end of the Heceta Bank complex, along with other abbreviated transects between these two sites. Depth contours are at 50-m intervals. (b) Wind forcing for the May–August period of 2001, as observed at the NOAA NDBC buoy 46050 (www.ndbc.noaa.gov/station_page.php?station = 46050). (c) Wind forcing for the May cruise, as observed from sensors mounted on the R/V *Thomas G. Thompson*. (d) Same as Figure 1c, but for the August cruise. Wind arrows in Figures 1b–1d scale to the red arrow in Figure 1d, which represents a 10 m s^{-1} due southward wind. Southward winds represent upwelling-favorable conditions. Horizontal lines in Figures 1c and 1d show the durations of the cross-shelf sections shown in later figures, with red segments representing the Cascade Head sections, and green segments representing the Cape Perpetua sections.

windows were cleaned daily. Beam-C was related to POC concentration by calibration against discrete samples collected from the sample stream and analyzed for POC by standard methods (Figure 2b). The POC:beam-C relationships are complicated. Beam-C and POC were highly correlated during both May and August (Figure 2b) but the May calibrations by *Karp-Boss et al.* [2004] yield a significantly different slope and intercept than the August calibrations. There are many reasons to expect that either slope or intercept may be variable in this setting as the relationship between beam-C and POC will vary with the composition and properties of the particles in the water [*Zaneveld*, 1973; *Pak and Zaneveld*, 1977; *Zaneveld and Pak*, 1979]. On the basis of the regression for the May data, many areas, particularly in the middle of the water column at the shelf break, have negative POC values, which we do not believe are realistic. We therefore assigned two somewhat arbitrary linear relationships between POC and beam-C for the ranges with 0 $m^{-1} \leq$ beam-c $\leq$ 0.4 m^{-1}, and beam-c > 0.4 m^{-1}. We discuss the significance of these calibration differences in error analysis below.

[12] Velocity data were collected using 150-kHz shipboard acoustic Doppler current profiler (ADCP), sampled at 5-s and 4-m-depth bins, and subsequently averaged over

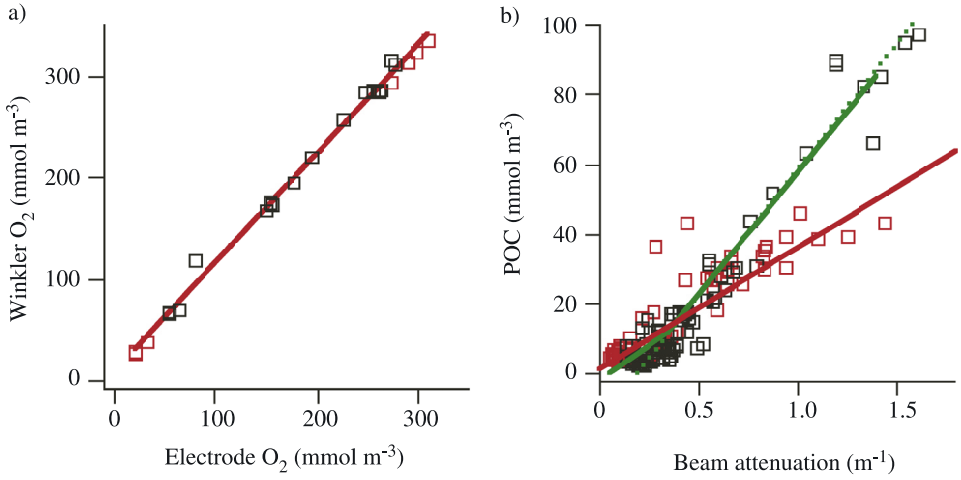

Figure 2. (a) Illustration of the calibration relationship between in situ electrode-based O_2 measurement and Winkler titration-based measurement of corresponding discrete samples (Winkler $[O_2]$ = 1.075 × electrode $[O_2]$ + 9). Calibration relationship is the same for the May (black symbols) and August data (red symbols). (b) Illustration of the calibration relationship between in situ transmissometer-based beam-C measurements and particulate organic carbon (POC) measurements in discrete samples. The two-section green solid line represents the two-part calibration of the May data that we believe is most applicable to the high and low ranges of beam-C and POC (POC = 43 × beam-C − 2 for beam-C ≤ 0.4; POC = 70 × beam-C − 13 for beam-C > 0.4); the dashed green line is the simple linear regression of all the May data, as in work of *Karp-Boss et al.* [2004] (POC = 71.5 × beam-C −13). The solid red line is the simple linear regression of all the August data (POC = 34.5 × beam-C + 1.5).

3 min. As the shoreline is essentially aligned in the N-S direction, we used the northward (v) component of these measurements to determine alongshore transport. *Perlin et al.* [2005a, 2005b] demonstrated that tidal velocities fluctuations were generally significantly smaller than mean alongshore flow and could be neglected to a certain degree for a 2D analysis. Velocities were extrapolated to the surface from the shallowest direct measurements assuming a 1° m^{-1} rotation due to Ekman veering. Velocities were extrapolated to the seafloor using the law-of-the-wall approach. Velocity data were interpolated onto SuperSucker's path, giving an estimate of alongshore velocity for each O_2 and POC measurement. Alongshore advective fluxes of O_2 and POC were calculated simply by multiplying the v velocity by their concentrations.

[13] When necessary, quantities were gridded to provide uniformly spatially weighted coverage across the sections. We created grid-cells that had horizontal and vertical dimensions of 140 and 1 m, respectively. Grid cells were filled with weighted averages of nearby measurements. Weighting was assigned to adjacent measurements on the basis of the inverse squared reduced distance, where the reduced distance was calculated as the square root of the sum of the reduced x and z distances from the grid cell. Reduced x and z distances were determined by dividing the actual distances (in meters) by 70 and 0.5 m, respectively. Data with reduced distances of more than 30 were not considered, and grid cells that were not bracketed in both dimensions by actual measurements were not filled. This resulted in grids that preserved the high variability seen in the ungridded data, but allowed smooth, uniformly weighted interpolation into unsampled regions.

3. Results

[14] We completed cross-shelf measurement sections at Cape Perpetua in late May (Figure 3) and mid-August (Figure 4) of 2001. These cross-shelf sections took ~1.5 days to complete, nearly synoptic in relation to the 75-day interim. Oxygen concentrations show the extreme variability typical of this setting, ranging from over 370 mmol m^{-3} (>100 mmol m^{-3} above saturation with respect to the atmosphere [*Garcia and Gordon*, 1992]) in surface waters, to less than 60 mmol m^{-3} (below most canonical definitions of hypoxia [e.g., *Richardson and Jorgensen*, 1996; *Rabalais et al.*, 2002; *Grantham et al.*, 2004] in near-bottom waters. While the high, near-surface O_2 concentrations are similar in May and August, there is markedly less O_2 in subsurface waters in August than in May. The minimum concentration observed in August is 23 mmol m^{-3} near the bottom (compared with 60 mmol m^{-3} in May), and the low-O_2 waters in August rise much farther up in the water column and across the shelf than in May.

[15] POC is likewise variable. Maxima, seen in near-surface waters, exceed 50 mmol m^{-3}, regardless of transmissometer calibration uncertainties, while the low values correspond to clear-water absorption and are at or below POC detection limits. Like the O_2 distributions, near-surface POC values are high and similar in May and August. Unlike O_2 distributions, which decrease nearly monotonically with depth throughout the sections, POC shows a secondary

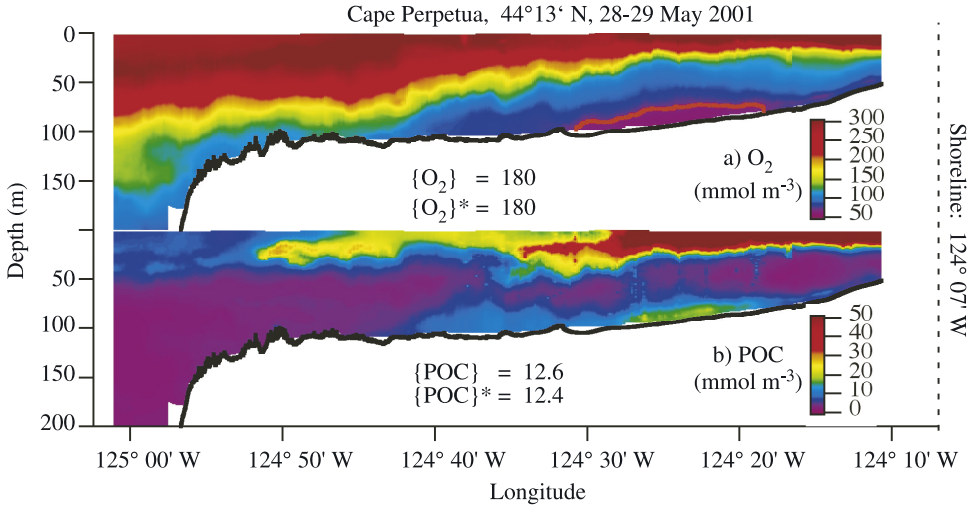

Figure 3. Cross-shelf distributions of calibrated (a) O_2 and (b) POC concentrations for the section completed at Cape Perpetua on 28–29 May 2001, uniformly spatially gridded following the routine described in section 2. Over 100,000 measurements were compiled in these gridded representations of the data. The thick red contour shows the location of the hypoxic horizon: O_2 concentrations in waters below this contour are <70 mmol m^{-3}. The vertical dashed line at the right of the figure shows the location of the shoreline at this latitude. The cross-shelf section was completed in about 40 hours. Measurements span the water column from ≤2 m below the surface, to ≤2 m from the bottom. Two average values of the POC and O_2 data are presented, each in brackets: The first is the average of all the data contained between the longitudes of the 50- and 180-m isobaths. The second, denoted with an asterisk, is the average of all data contained between the longitudes of the 35- and 200-m isobaths.

maximum near the bottom, likely due to sinking of surface-produced particulate material that is kept in suspension by the high turbulence observed in the bottom boundary layer [*Moum et al.*, 2005; *Perlin et al.*, 2005a]. While we cannot exclude the contribution of sediment resuspension to near-bottom beam-C, transmissometer calibrations in the BBL and upper water column were similar, and near-bottom shear would not be sufficient to resuspend the coarse sandy sediments of the OR shelf [*Karp-Boss et al.*, 2004]. These near-bottom POC concentrations can exceed 20 mmol m^{-3}.

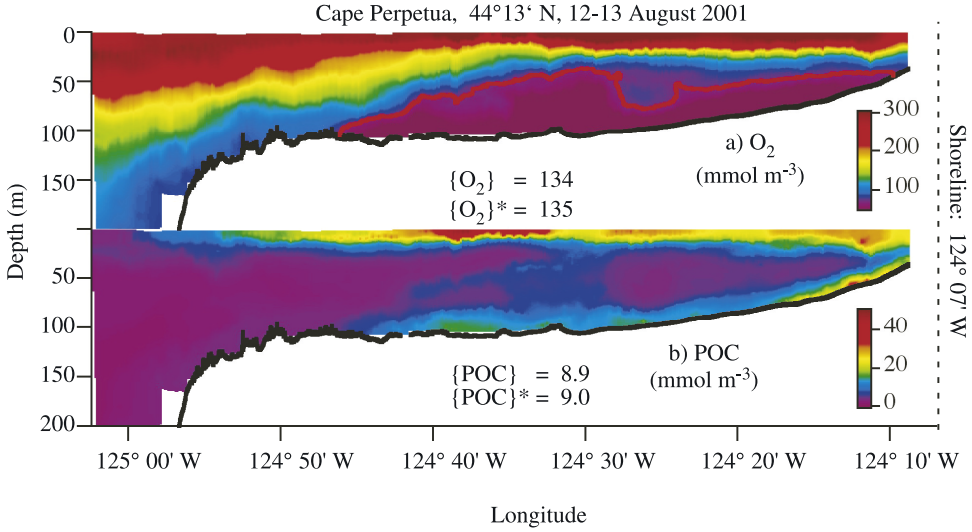

Figure 4. Same as Figure 3, but for the section across Cape Perpetua completed on 12–13 August.

In seeming contrast to the seasonal decrease in subsurface O_2 concentrations, subsurface POC values in August are actually higher than in May.

4. Discussion

[16] A few qualitative but, we believe, robust, inferences can be made from observation of the distributions shown in Figures 3 and 4. First, supersaturated surface O_2 concentrations must be a result of rapid, ongoing photosynthetic production; only about 30% of the observed supersaturation can be due to warming. For reasonable gas exchange rates (2–3 m day; see below) and conservatively deep estimates of mixed layer depths (20–30 m), the characteristic time for equilibration by gas exchange is 7–15 days. The observed supersaturations could not persist over the course of the summer if they were simply remnants of some previous productivity event. Second, the May–August decrease in deep-water O_2 seems not to be a simple result of respiration. Deep-water POC stocks appear to increase over time, and stoichiometric calculations suggest that the observed BBL POC in May would have been more than enough to entirely deplete BBL O_2. The lack of clear relationships between stocks of, and changes in, POC and O_2 suggests that there is some decoupling between POC and O_2 despite the connections between their production and diagenesis. Third, hypoxic near-bottom water is present on the shelf in both May and August. By August the hypoxic region has expanded to cover nearly the entire cross-shelf expanse, and the hypoxic boundary has moved up to within 50 m of the surface at mid-shelf depths. These widespread hypoxic conditions have developed in the absence of anomalous low-O_2 water at the shelf break, and apparently without significant mass mortality events [*Grantham et al.*, 2004].

[17] These observations paint a picture of a system with high ongoing O_2 and POC productivity in surface waters, and continuous export of POC to depth where waters are on the hypoxic threshold throughout the upwelling season. Once exported to depth, some POC is undoubtedly respired, but there is a decoupling between O_2 and POC distributions that is unexplained. In the following sections we quantify the cross-shelf balances of O_2 and POC, make estimates of the net average rate of O_2 and POC production, and finally speculate about the fate of the POC production.

4.1. Oxygen Budget

[18] Time- and space-dependent distributions of O_2 and POC are governed by continuity,

$$\frac{\partial [O_2]}{\partial t} = \nabla(\mathbf{k} \bullet \nabla[O_2] - \mathbf{v} \bullet [O_2]) + R_{O2}, \qquad (1)$$

where $[O_2]$ represents the time- and space-dependent concentration of O_2 (mmol m^{-3}), **k** and **v** represent the combined x, y, and z terms of eddy diffusivity (m^2 s^{-1}) and advection (m s^{-1}), respectively, and R_{O2} (mmol m^{-3} s^{-1}) represents the time- and space-dependent net generation of O_2 (which will be negative if there is net consumption). Given appropriate knowledge of **k**, **v**, and boundary conditions, the distributions of O_2 might be used to constrain an inverse model that would ultimately yield spatially and temporally resolved distributions of R_{O2} which could be subsequently integrated to determine shelf-wide net production rates.

[19] Our ultimate goal is determination of net shelf-wide production, and we chose a simplified approach of calculating the time-dependent balance of the cross-shelf integrated water column O_2 content. This has several features: (1) A vertical domain of the sea surface to the seafloor precludes effects of vertical mixing; (2) the inshore boundary prevents net transport of any kind to the east, and horizontal advection is limited to net exchange at the shelf break and alongshore advection; and (3) air-sea exchange and benthic consumption can be treated as sources and sinks in a macroscopic O_2 budget.

[20] We further chose to limit our analysis to a control volume made up of the section across the shelf at Cape Perpetua with some differential (e.g., 1 m) north-south (y) dimension. This is a natural choice as it is more representative of the conditions of Heceta Bank than is the section at Cascade Head, and, owing to its location at the downstream end of the bank, is more likely to tell us about off-shelf exchange than would a more centrally located section. By making the further assumptions that advection dominates mixing in the horizontal, that alongshore transport can be approximated by the northward (v) component of the velocity field, and that the time-rate-of-change can be approximated by simple difference, the budget reduces to

$$\begin{aligned}\frac{\Delta \int_{x=sl}^{x=sb}\int_{z=b}^{z=0}[O_2]dzdx}{\Delta t} &= \int_{x=sl}^{x=sb}\int_{z=b}^{z=0} R_{O2}dzdx \\ &+ \int_{x=sl}^{x=sb} k_{ge}\left([O_2]_{sat} - [O_2]_{surf}\right)dx \\ &+ E\left([O_2]_{up} - [O_2]_{off}\right) \\ &+ \frac{-\Delta \int_{x=sl}^{x=sb}\int_{z=b}^{z=0} v[O_2]dzdx}{\Delta y} + \int_{x=sl}^{x=sb} Bdx, \qquad (2)\end{aligned}$$

where k_{ge} is the gas exchange rate (m s^{-1}); E is the rate of wind driven upwelling transport (m^2 s^{-1} [*Lentz*, 1992, *Perlin et al.*, 2005a, *Hales et al.*, 2005b]); v is the northward component of velocity (m s^{-1}), and B is the rate of benthic consumption of O_2 (mmol m^{-2} s^{-1}; hereafter assumed constant). The integration limits *sb* and *sl* refer to the positions of the shelf break and shoreline, respectively, while the integration limit *b* refers to the depth of the seafloor at a given longitude. Dividing the above equation by the cross-sectional area of the section at Cape Perpetua, A_{CP} (5.9×10 m^2) leads to

$$\begin{aligned}\frac{\Delta\{[O_2]\}}{\Delta t} &= \{R_{O2}\} + \frac{\int_{x=sl}^{x=sb} k_{ge}\left([O_2]_{sat} - [O_2]_{surf}\right)dx}{A_{CP}} \\ &+ \frac{E\left([O_2]_{up} - [O_2]_{off}\right)}{A_{CP}} + \frac{-\Delta \int_{x=sl}^{x=sb}\int_{z=b}^{z=0} v[O_2]dzdx}{\Delta y} + B', \qquad (3)\end{aligned}$$

Table 1. Summary of the Discrete O_2 Budget

Budget Term	Estimation Method	Value, mmol m^{-3} d^{-1}	Uncertainty, mmol m^{-3} d^{-1}	Uncertainty Estimation Method
Temporal change	difference between 5/28 and 8/12 cross-shelf integrated O_2 at CP divided by 75 days	−0.61	±0.12	±3% uncertainty in May and August integrated O_2
Air-sea exchange	cross-shelf integrated instantaneous gas exchange flux, using cubic dependence on TGT DAS wind speed	−0.64	−0.17–+0.09	comparison of cross-shelf integrated flux estimated with various combinations of winds from NDBC 46050, 2nd-order dependence on wind, etc.
Cross-shelf transport	mean Ekman transport multiplied by difference between source and surface water concentrations	−0.66	±0.17	uncertainty in Ekman flow propagated by uncertainty in source and surface water O_2 concentrations
Alongshore transport	difference between cross-shelf integrated O_2 fluxes at CH and CP, divided by distance between CH and CP	−1.3	−2.3–+1.3	extreme ranges in observed alongshore water transport; max. uncertainties in average O_2
Consumption in sediments	*Hartnett and Devol* [2003]	−0.10	±0.10	100% uncertainty
Net production	temporal change minus sum of remaining terms	2.1	−1.3–+2.3	propagation of above uncertainties

where the brackets denote average properties, and B' is the average benthic consumption flux divided by the average depth of the water column across this section. The average rate of O_2 production, $\{R_{O2}\}$, can be determined by rearranging equation (3).

[21] This approach is conceptually similar to that employed by *Emerson et al.* [1997, 1995, 1991] for analyses of single-location vertical profiles in the subtropical and subarctic North Pacific. Our analysis benefits from several unique features of this data set. First, intensive sampling and cross-shelf coverage means that our two time-point estimates of standing stock have little sensitivity to short-term temporal variability, or to aliased spatial variability. Second, because our data coverage spans nearly the entire water column, we have no uncertainty associated with assignment of a deep boundary for our calculations, and no mixing flux through that boundary. Third, advection, both in the alongshore and across-shelf dimensions are well constrained. In the case of the former, we have direct estimates of v from ship-board ADCP data. In the case of the latter, cross-shelf transport is known to be consistently onshore at depth, and offshore at the surface. Finally, we have good data coverage upstream of our Cape Perpetua sections, allowing estimation of the alongshore advective flux-divergence term. Determination of each term is described below, and the results summarized in Table 1.

[22] The temporal rate of change of average O_2 concentration is one of the easier terms to quantify. It is determined from the difference of concentrations in August (134 mmol m^{-3}; average of gridded section shown in Figure 4a between 50- and 180-m isobaths) and May (180 mmol m^{-3}; average of gridded section shown in Figure 3a), divided by the elapsed 75 days, for a change of O_2 in the system of −0.61 mmol m^{-3} d^{-1}. Uncertainties in this term are small. The most significant has to do with short-term variability in O_2 concentration. The occupations of this section in May and August might have captured some day-to-day variability such that differencing these two snapshots separated in time by 2.5 months is not a perfectly reliable estimate of the longer-term decrease in O_2. To estimate the magnitude of this uncertainty, we turn to a series of eight cross-shelf measurement sections at the northernmost, narrow-shelf location at Cascade Head during a 7-day period in May (auxiliary material[1] Figures S1a and S1b). Despite large internal variability present in each section, the averages of each section are remarkably constant, ranging from 154 to 161 mmol m^{-3}, with an average of 158 mmol m^{-3}, implying a maximum ±2.5% uncertainty. This result is further borne out by comparison of an abbreviated mid-shelf measurement section in May at Cape Perpetua (auxiliary material Figure S2) to the full section of Figure 3. Average O_2 concentration on this shorter section is 150 mmol m^{-3}. Average O_2 concentration on the prior section within the limits of the shorter section is 152 mmol m^{-3}. The difference (1.3%) is well within the uncertainties based on the Cascade Head sections. Another uncertainty results from an incomplete shore-to-shelf-break longitudinal range. This can be assessed somewhat by examining the difference between the average concentrations within the 50- to 180-m isobath limits and those calculated on longer sections. Cross-shelf averages are no more than 2 mmol m^{-3} different when limited to either the 50- to 180- or 35- to 200-m isobaths. We thus feel that a 3% uncertainty in the cross-shelf averaged O_2 concentrations is a conservative error estimate, and this results in uncertainty of ±0.12 mmol m^{-3} d^{-1}.

[23] Gas exchange is also fairly easy to estimate. We took the difference between the observed surface O_2 concentrations from the raw data of Figures 3 and 4 and the saturation concentrations calculated from the relationship of *Garcia and Gordon* [1992] for the coincident temperature and salinity (Figures 5a and 6a), and at each point multiplied that difference by the gas exchange coefficient determined from instantaneous wind speed collected from shipboard sensors (Figures 5b and 6b) gas-transfer velocity parameterization of *McGillis et al.* [2001], corrected appropriate to O_2 and in situ temperature, to yield an instantaneous gas exchange flux. This was then integrated across the shelf, and divided by the cross-shelf section area. Gas exchange

[1] Auxiliary material is available at ftp://ftp.agu.org/apend/gb/2005gb002517.

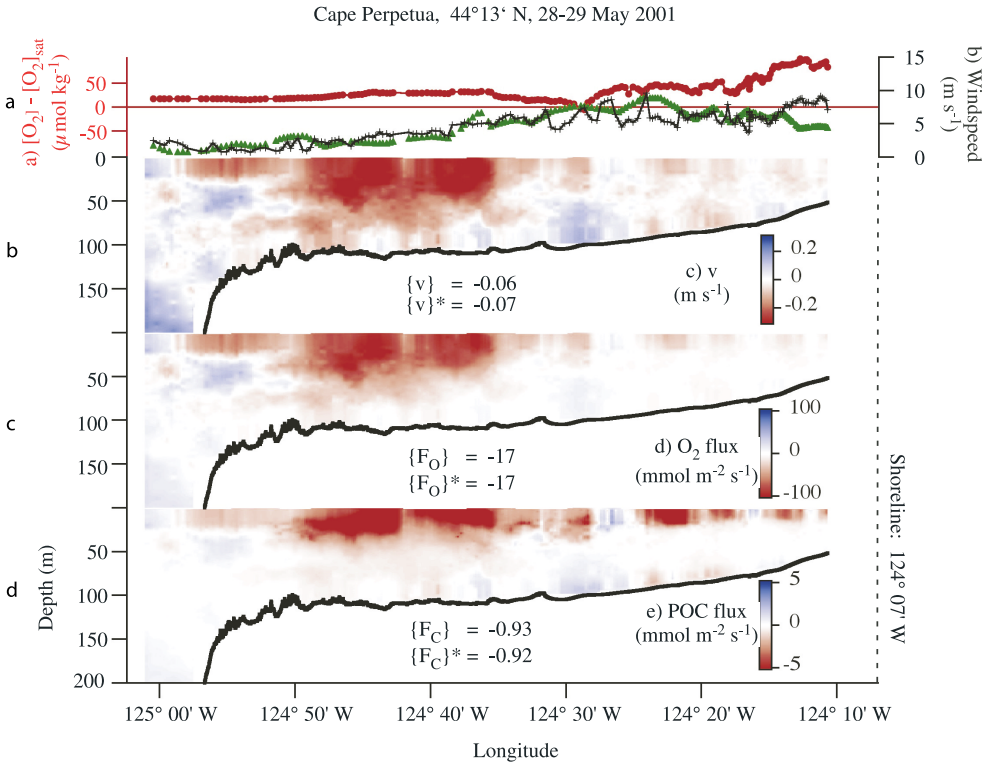

Figure 5. Additional information used for the O_2 and POC budgets at Cape Perpetua in May. (a) Surface O_2 supersaturation (solid red circles), calculated from the raw, ungridded surface concentration data, and the solubility relationship of *Garcia and Gordon* [1992]. (b) Wind speed data from the ship-based sensors (black crosses) and the NDBC 46050 mooring-based sensors (green triangles), at the time of each surface saturation determination in Figure 5a. (c) Alongshore velocity distributions, determined by interpolating the ship-based ADCP v data onto the position of the profiling sampler at each measurement time, and gridding that result using the approach described in section 2. (d) Alongshore O_2 flux, determined by gridding the product of the ungridded ADCP and O_2 concentration data. (e) Alongshore POC flux, determined similarly to the O_2 flux. Average values of the gridded data in brackets are as in Figures 3 and 4.

resulted in a loss from the system of −0.65 and −0.63 mmol m^{-3} d^{-1} for the May and August sections, respectively. We chose −0.64 mmol m^{-3} d^{-1} as the average loss from the system by gas exchange over the 75-day interval. Uncertainty estimation for this term is related to the method for calculating the gas exchange coefficient, and the choice of calculating fluxes from products of instantaneous-wind-based gas-exchange coefficients and supersaturations versus longer-term averages of these two. We considered the range of estimates that would result from all combinations of several different factors. The smallest calculated loss from the system due to gas exchange is −0.55 mmol m^{-3} d^{-1} (using section-average ship-based wind speed, the *McGillis et al.* [2001] wind speed dependence and section-average supersaturation) and the greatest calculated loss from the system is −0.81 mmol m^{-3} d^{-1} during the August section (using instantaneous wind speed measured at the nearby NDBC 46050 buoy, the *Wanninkhof* [1992] wind speed dependence, and section average supersaturation). We thus feel that the most robust estimate of the uncertainties in this term are −0.17 and +0.09 mmol m^{-3} d^{-1} for August and May, respectively (Table 1).

[24] Cross-shelf exchange is limited to wind-driven offshore Ekman transport in surface waters, and compensating upwelling flow at depth. *Lentz* [1992] and *Perlin et al.* [2005a], using completely independent methods, estimated upwelling transport at 0.25 m^3 s^{-1} and 0.2 m^3 s^{-1}, respectively, per meter of coastline. Assuming continuity in the upwelling and offshore flows, we use the difference between the upwelled and surface water concentrations at the shelf break to estimate this net flux. At the shelf break, upwelled water (in the density range 26.5 to 26.68) has O_2 concentrations ranging from 70 to 110 mmol m^{-3}; water from the surface to 30 m depth has O_2 concentrations ranging from 280 to 300 mmol m^{-3}. These concentrations are similar in both May and August. We chose the midpoints in these respective concentration ranges, and multiplied their difference by the average of the *Lentz* [1992] and *Perlin et al.* [2005a] upwelling flows. This leads to estimation of an average loss of −0.66 mmol O_2 m^{-3} d^{-1}. Uncertainties are simply estimated by examining extreme ranges in the concentration differences and transport rate: The minimum loss from the system is −0.50 mmol m^{-3} d^{-1};

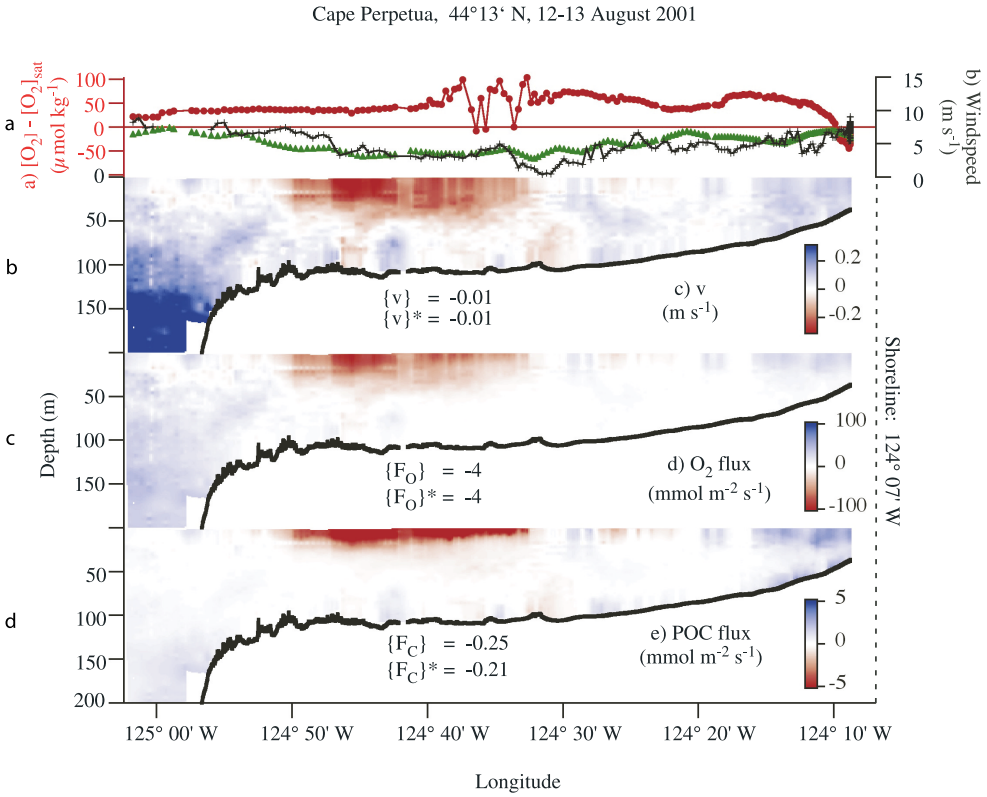

Figure 6. As Figure 5, but for the section at Cape Perpetua completed on 12–13 August.

the maximum is −0.84 mmol m^{-3} d^{-1}. We estimate the uncertainty in this term at ±0.17 mmol m^{-3} d^{-1}.

[25] Alongshore transport is a large term in the O_2 budget that is difficult to constrain. We projected the v component of the ADCP-based velocity (Figures 5c and 6c) onto our high-resolution data, and then calculated instantaneous fluxes from the product of v and the O_2 concentration at each measurement point (Figures 5d and 6d). The net effect of alongshore transport on the Cape Perpetua section is a result of the alongshore flux divergence, constraint of which requires estimation of the alongshore flux gradient. This has many complicating factors, the first of which is the limited coverage of alongshore flux data. Unfortunately, we only have adequate cross-shelf coverage at the Cascade Head site in addition to Cape Perpetua, which requires us to calculate the alongshore flux divergence using an "upstream-difference" approximation of the divergence. Imposition of a flux divergence calculated by difference between Cape Perpetua and Cascade Head-on Cape Perpetua implicitly assumes that the flux divergence is constant between those two locations. The second problem with this calculation is the large temporal variability of the alongshore fluxes, shown by the series of sections at Cascade Head (auxiliary material Figures S1a, S1b, and S3), even when integrated across the shelf. This confounds further the calculation of alongshore flux divergence. Should flux divergences be estimated from the two Cape Perpetua and Cascade Head sections most closely spaced in time? Or should the comparison be made between sections separated by the mean transit time between the two sections (about 10 days, given the net alongshore transport rates estimated below, and a rough estimate of the volume bounded by the shore and shelf break and the Cascade Head and Cape Perpetua sections)?

[26] This calculation would be all but impossible if not for three features of the system. The first is the fact that mean transport is southward, driven by the prevailing equatorward wind forcing. When integrated across the Cascade Head section, the net transport is about −0.4 Sv, while the maximum mean velocity (−0.28 m s^{-1}) correspond to net transport of −0.7 Sv. These transport estimates are in excellent agreement with those given by *Castelao and Barth* [2005], lending confidence to our data analysis procedures. The second is that there is continuity of alongshore water transport between these two sections inshore of the shelf break. This is supported by the observed coherence in alongshore velocities over the shelf over long distances [*Kundu and Allen*, 1976; *Kosro*, 2005]. Potential vorticity conservation makes large net transport across the shelf break highly unlikely [*Gill*, 1982], so it is probable that net flows through the Cape Perpetua and Cascade Head sections are similar. This is supported by the observation that water fluxes through the Cascade Head section on 27 May are about the same as they are through the Cape Perpetua section on 28–29 May (both about 0.35 Sv), an interval when wind forcing was relatively constant. The third is the fact that the O_2 content of the Cape Perpetua section is greater than the O_2 content of the Cascade Head section in every observation. The differences between the

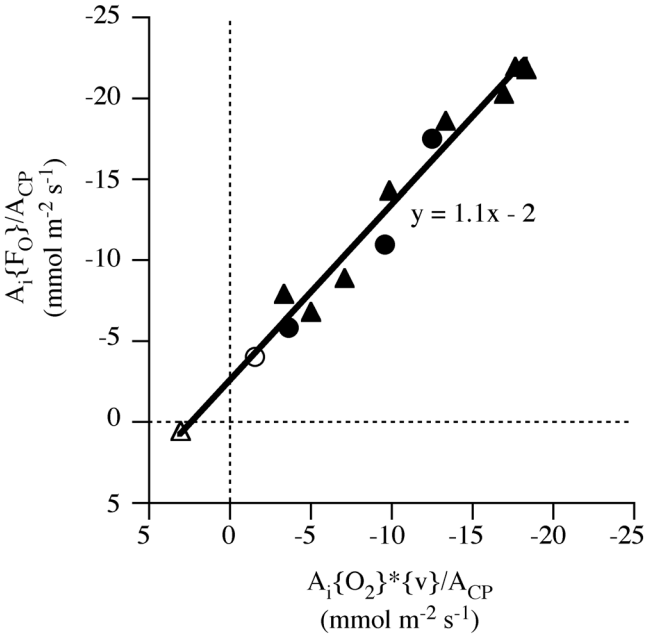

Figure 7. Relationship between area normalized section-averaged alongshore O_2 flux ($\{F_O\}$) and the product of section-averaged O_2 concentration ($\{O_2\}$) and alongshore velocity ($\{v\}$). Circles represent Cape Perpetua sections. Triangles represent Cascade Head sections. Solid symbols are May sections. Open symbols represent August sections.

sections in May and August, 22 ± 10 and 14 ± 8 mmol m^{-3}, respectively, are both significantly greater than zero.

[27] These suggest a system where low-O_2 water flows in from the north, and the same amount of water, but with a higher O_2 content, flows out to the south. This simplistic view would not hold if there were complicated relationships between the O_2 concentration and velocity distributions at either section. If, for example, velocity and O_2 concentration were highly correlated at the Cascade Head section, high-O_2 water would be preferentially transported southward toward Cape Perpetua. If the two parameters were then anticorrelated at Cape Perpetua, low-O_2 water would be preferentially transported away to the south. The absence of this sort of condition is illustrated by the relationship between the area-normalized alongshore flux and the area-normalized product of section-averaged velocity and section-averaged O_2 concentration illustrated in Figure 7. If there were significant correlations or anticorrelations between the velocity and O_2 distributions, a simple correlation between average of the product of velocity and concentration and the product of their averages would not be expected. A strongly linear relationship with a slope slightly exceeding unity and a small negative offset is in fact seen. This relationship holds for both Cape Perpetua and Cascade Head sections, in both May and August intervals.

[28] This allows estimation of the mean, and constraint of the extreme, alongshore flux divergence using section-average properties. For a mean transport of −0.43 Sv and a mean concentration difference between the two sections of 18 mmol m^{-3}, the average alongshore flux divergence results in a loss of O_2 from the Cape Perpetua of −1.3 mmol m^{-3} d^{-1}. We can likewise estimate the extreme ranges in this term: For a transport of −0.67 Sv, and a maximal concentration difference of 32 mmol m^{-3}, the alongshore flux divergence term is −3.6 mmol m^{-3} d^{-1}; for a lower-bound transport of 0 Sv, this term would be 0 mmol m^{-3} d^{-1}. We thus conclude that the alongshore flux-divergence term has uncertainties of +1.3 and −2.3 mmol m^{-3} d^{-1} to incorporate the limits determined above.

[29] Benthic consumption of O_2 is largely unconstrained. We are aware of no published benthic flux study off Oregon. Off the Washington coast, benthic fluxes result in a net loss of O_2 from the water column of about −0.1 mmol m^{-3} d^{-1} when normalized to the average shelf depth [*Hartnett and Devol*, 2003]. Recent preliminary results off Oregon suggest similar benthic O_2 consumption rates (C. Reimers, personal communication, 2005), and we will use the *Hartnett and Devol* [2003] estimate here. We arbitrarily assign an uncertainty of 100% (±0.1 mmol m^{-3} d^{-1}) to this flux term.

[30] Before proceeding with calculation of the net O_2 productivity, we reiterate that the uncertainties are the largest we could assign. It is difficult to estimate how many standard deviations they represent, but as they span the maximum limits of the terms above, they are probably greater than 3-sigma uncertainties, and the error bars given represent better than 95% confidence limits.

[31] Average net O_2 productivity is calculated from the temporal change in the system, minus the sum of all the other terms constrained above, as detailed in equation (3) and listed in Table 1. The May–August rate of change in O_2 content at Cape Perpetua is −0.61 mmol m^{-3} d^{-1}, while the other best-estimate terms amount to a net flux of −2.7 mmol m^{-3} d^{-1}. In order for the system to be in balance and equation (3) to hold, there must be an average net O_2 production of 2.1 mmol m^{-3} d^{-1}. As there is no reason to expect the uncertainties in the terms that go into this calculation to be correlated or anticorrelated, we calculate the uncertainty in this production term by simple error propagation of the (extreme) uncertainties given in Table 1. This leads us to assign uncertainties of −1.3 mmol m^{-3} d^{-1} to +2.3 mmol m^{-3} d^{-1}. Confidence in the above estimate is given by making two crude comparisons. First, a Lagrangian-based calculation of the productivity that a parcel of shelf water would experience in its transit from Cascade Head to Cape Perpetua, which is dominated by alongshore flow, is about 2 mmol m^{-3} d^{-1}, given the average concentration difference between the sections and the mean alongshore transit time. Second, an oversimplified budget for nitrate distributions [*Hales et al.*, 2005b; B. Hales, unpublished data, 2001] yields similar net productivity estimates.

[32] This is a large net productivity, about 200 mmol O_2 m^{-2} d^{-1} when integrated over the water column (∼100 m), and we need to place it in context with other productivity estimates. *Small and Menzies* [1981] and *Dickson and Wheeler* [1995] reported daylight primary productivity of 800–4500 mmol O_2 m^{-2} d^{-1} (scaled to a 12:12 L:D cycle, 30-m euphotic layer, and assuming a photosynthetic quotient (PQ) of 1.5 [*Hedges et al.*, 2002; *Anderson and*

Table 2. Summary of the Discrete POC Budget

Budget Term	Estimation Method	Value, mmol m^{-3} d^{-1}	Uncertainty, mmol m^{-3} d^{-1}	Uncertainty Estimation Method
Cross-shelf transport	mean Ekman transport multiplied by surface POC at shelfbreak; POC in upwelled waters assumed = 0	−0.030	−0.003–+0.030	extreme ranges in observed surface and upwelled POC, extreme uncertainties in calibration, and uncertainty in Ekman transport
Alongshore transport	difference between mean cross-shelf integrated POC fluxes at CH and CP divided by distance between CH and CP	−0.27	−1.02–+0.27	extreme ranges in observed alongshore POC flux, extreme uncertainties in calibration
Temporal change	difference between 5/28 and 8/12 cross-shelf integrated POC at CP, divided by 75 days	−0.05	−0.10–+0.05	extreme ranges in observed average POC at CP, accounting for short-term variability, and calibration uncertainties
Consumption + burial in sediments	*Hartnett and Devol* [2003]	−0.15	±0.15	100% uncertainty
Net production	stoichiometric conversion of O_2 production with PQ = 1.5	1.4	−0.9–+1.2	uncertainties in P_{O2} propagated by uncertainty in PQ ($1.3 \leq PQ \leq 1.5$)
Budget imbalance		−1.0	−0.4–+0.7	propagation of above uncertainties, accounting for correlated errors

Sarmiento, 1994; *Bender et al.*, 1992]), based on daylight ^{14}C incubations of Oregon shelf water. These rates are similar to those compiled by *Perry et al.* [1989] for the nearby, similar, Washington shelf during summer upwelling conditions. We have no sure way of converting this primary productivity to a comparable net community productivity, but will simply remark that our section-average net O_2 productivity is 5–25% of euphotic-zone primary productivity in this setting, and that high f-ratios are common for coastal phytoplankton assemblages [*Harrison et al.*, 1987; *Kokkinakis and Wheeler*, 1987].

4.2. POC Budget

[33] The POC budget is simpler than the O_2 budget because of the absence of gas exchange as a viable transport pathway, and because POC production must be stoichiometrically related to the O_2 production determined in the previous section. River input of terrestrially derived carbon is negligible during summer. Thus the POC budget is as follows:

$$\frac{\Delta\{[POC]\}}{\Delta t} = \frac{\{R_{O2}\}}{PQ} + \frac{E\left([POC]_{up} - [POC]_{off}\right)}{A_{CP}} + \frac{-\Delta \int_{x=sl}^{x=sb} \int_{z=b}^{z=0} v[POC]dzdx}{\Delta y} + B'', \quad (4)$$

where PQ is the stoichiometric photosynthetic quotient relating the rate of POC production to the rate of O_2 production, and B'' is the average consumption of POC by burial and respiration in the sediments. As the process is similar to that we followed in constraining the O_2 budget we will not belabor the calculation of each term in this balance. Rather, we refer the reader directly to Table 2, where the results of this exercise are summarized, and discuss them briefly below.

[34] Despite the high average POC productivity (1.4 (−0.9/+1.2) mmol m^{-3} d^{-1}), there is no significant change in POC standing stock between May and August (−0.05 (−±0.05) mmol m^{-3} d^{-1}). Cross-shelf Ekman transport (−0.03 (−0.003/+0.03) mmol m^{-3} d^{-1}) is only a small loss. *Hartnett and Devol* [2003] report that benthic mineralization of carbon consumes at most 0.15 mmol C m^{-3} day, and that sediment carbon burial amounts to only a few percent of the total benthic mineralization. The most significant identified loss term is alongshore transport, (−0.27 (−1.0/+0.27) mmol m^{-3} d^{-1}). Even this is relatively small in the budget owing to the small differences between Cascade Head and Cape Perpetua POC concentrations. All of these terms together do not completely account for the production of POC, with a residual term equivalent to −1.0 (−0.4/+0.7) mmol m^{-3} d^{-1}, or 73% of the best-estimate POC production, required to balance the budget.

[35] The greatest contribution to uncertainties in this calculation not inherent in the discussion of the O_2 budget comes from the slightly more variable cross-shelf-averaged POC content (estimated at ±15%, given comparison of day-day variability in averaged concentrations at Cascade Head in (auxiliary material Figures S1a and S1b) and abbreviated Cape Perpetua sections (auxiliary material Figure S3), and the uncertainty due to the different beam-C versus POC calibrations discussed in section 2. For example, applying the August calibration to the May data at Cape Perpetua decreased the estimated average POC from 12.6 to 11.9 mmol m^{-3}, while applying the two-segment May calibration to the August data there increased estimated POC from 8.8 to 9.3 mmol m^{-3}. Even applying a +15% correction to the August data, and a −15% correction to the May data cannot result in a POC increase from May to August. Assigning the August calibration to the May

Table 3. Examination of the Residual Transport Term in Cases of Extremes in Alongshore Transport and Productivity

Case	POC Productivity[a]	Alongshore POC Transport[b]	'Residual' POC Transport[c]	Alongshore |Trans./Prod.|[d]	Residual |Trans./Prod.|[d]
Maximum alongshore water transport, Minimum productivity	0.82	−0.39 (+0.39/−0.78)	−0.35 (+0.78/−0.42)	0.48 (+0.52/−0.48)	0.43 (+0.51/−0.43)
Maximum alongshore water transport, Maximum productivity	3.7	−0.39 +0.39/−0.78)	−3.0 +0.78/−0.42)	0.11 +0.21/−0.11)	0.81 +0.11/−0.21)
Zero alongshore water transport, Minimum productivity	0.37	0	−0.24 ± 0.15)	0	.65 +0.35/−0.41)
Zero alongshore water transport, Maximum productivity	0.85	0	−0.72 ±0.16)	0	0.85 +0.15/−0.19)

[a]POC productivity calculated stoichiometrically from corresponding O_2 productivity: minimum productivity assumes PQ = 1.5; maximum productivity assumes PQ = 1.3 [*Redfield et al.*, 1963].

[b]Uncertainties in alongshore POC transport for fixed water transport determined from uncertainty in POC difference between Cascade Head and Cape Perpetua based on uncertainties in section-averaged POC concentrations.

[c]Uncertainties in residual transport determined by propagation of uncertainties in other terms.

[d]Uncertainties in ratios truncated such that ratios fall between 0 and 1.

Cascade Head data results in an average increase in estimated average POC of 30%, but in no case is the POC there greater than estimated at Cape Perpetua. These uncertainties are incorporated into the above-stated error estimates.

4.3. Off-Shelf POC Export

[36] For the best estimate of all parameters in the POC budget, the sum of alongshore- and residual-transport exports from the system is essentially equivalent to the net productivity, and the two terms each export a significant amount of POC from the system. What is less clear, owing to the large uncertainties, is how significant the alongshore and residual transport terms are relative to each other, and how significant each is individually relative to average production. Because productivity is determined from the O_2 balance, which depends strongly on alongshore transport, and because the residual transport is determined from the POC budget, which depends strongly on the productivity and the alongshore transport, the largest uncertainties in these calculations are highly correlated and largely self-canceling. We examined four extreme cases to constrain the limits of these relations: maximum and minimum productivity for maximum southward alongshore transport, and maximum and minimum productivity for zero alongshore transport. For each case, we take the alongshore water transport and POC productivity as fixed at extreme values, and then calculate alongshore and residual POC transport.

[37] These results are summarized in Table 3. For maximum alongshore water transport, and minimum O_2 productivity at that high transport, the POC productivity is 0.82 mmol m^{-3} d^{-1}. Alongshore POC transport in this high-flow condition is −0.39 (+0.39/−0.78 mmol m^{-3} d^{-1}, given uncertainties in cross-shelf averaged POC concentrations). In this case, the residual loss is −0.35 (+0.78/−0.42) mmol m^{-3} d^{-1}. Given the correlation of uncertainties in the two transport terms, their sum is always 0.74 mmol m^{-3} d^{-1}, and removes 91% of the productivity. On average, alongshore transport removes 48% of the net productivity, while the residual transport removes the remaining 43%. For maximum alongshore transport and maximum O_2 productivity, POC productivity is 3.7 mmol m^{-3} d^{-1}, and the residual transport is −3.0 (+0.78/−0.42) mmol m^{-3} d^{-1}. Again, as the uncertainties are correlated, the sum of residual and alongshore transport terms is always −3.4 mmol m^{-3} d^{-1}, and the two processes combine to remove 92% of the net productivity. In this case, however, the residual transport removes 81% of the productivity, while the alongshore transport removes 11%. For the case of zero alongshore water transport, residual loss accounts for 65 and 85% of the productivity in the high- and low-productivity cases.

[38] We summarize these results in the following way: Two processes, alongshore advective transport and some undefined residual loss, combine to remove 65−92% of the POC that is produced on the shelf. Except for one extreme case of maximum alongshore transport and minimum POC productivity, where residual and alongshore transport remove roughly equivalent amounts of POC, residual transport is responsible for most of the removal. In either pathway, POC is probably removed from the shelf to the deep ocean where it can sink to depths below seasonally upwelled waters. The bathymetry of Heceta Bank is such that the Cape Perpetua section is immediately upstream, in the mean flow sense, from the abrupt southern edge of the bank. Most of the alongshore flow through this section probably crosses the shelf break to the south, carrying the POC to regions where the bottom depths exceed 1000 m. If this material sinks to these depths, the end result is a long-term sequestration of carbon in the deep ocean. We cannot definitively conclude that most of the POC removal is occurring by some unspecified process, but the evidence is strong enough to require some discussion of what this process might be. In order for a transport process to remove a significant amount of POC from the system, that process must coincide with elevated concentrations of POC. There are essentially two locations that contain high POC concentrations: Near-surface waters and bottom-boundary layer (BBL) waters, which are high in POC because of surface production and near-bottom accumulation and resuspension, respectively. We have accounted for all transport and reaction processes of significance for a continuously upwelling system, and now discuss the possibility that temporal variability in the upwelling forcing may play a role in exporting POC from the system

[39] In a constantly upwelling system, schematically depicted in Figure 8a, equatorward alongshore winds drive

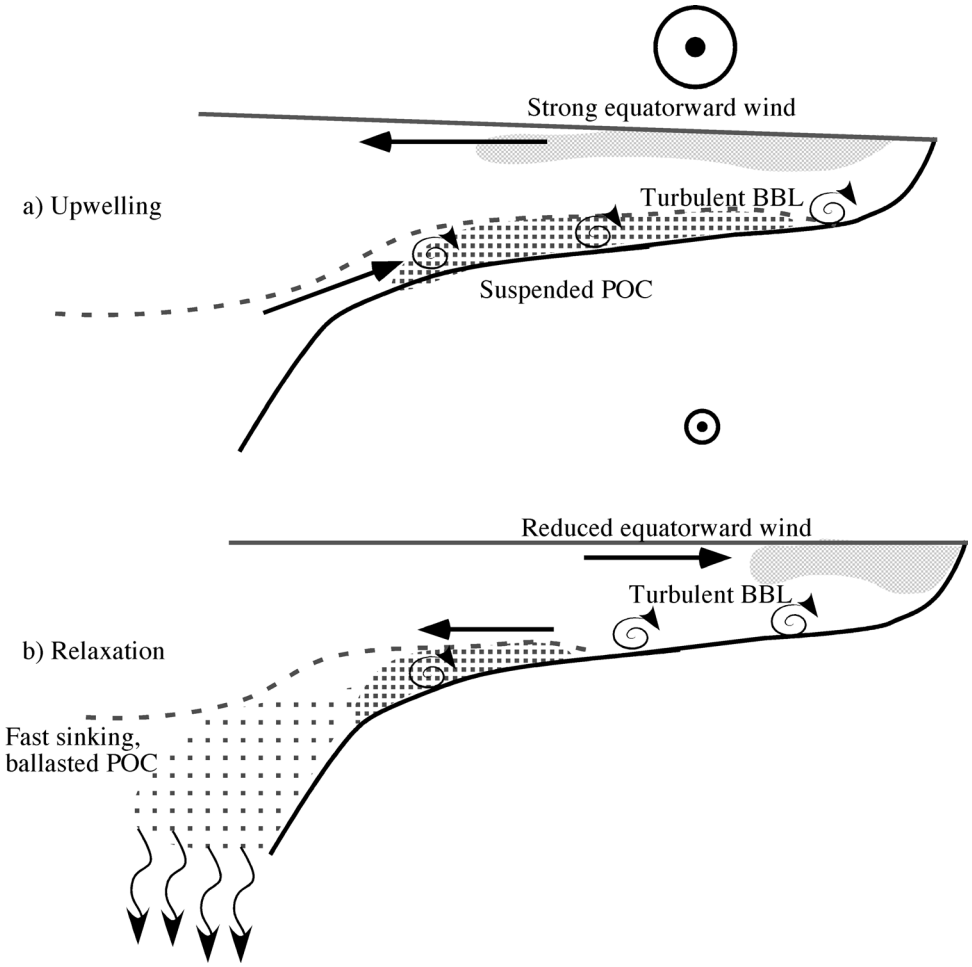

Figure 8. Schematic representation of simplified (a) upwelling and (b) relaxation conditions. Small near-surface dots represent newly photosynthetically produced POC. Larger near-bottom dots represent flocculated, ballasted POC.

net Ekman flow offshore and draw compensating flow up and onshore through the BBL from deep offshore isopycnals. The delivery of upwelled nutrients to the euphotic zone fuels photosynthetic POC productivity. If this condition persisted, POC stocks would increase with time; be transported out of the system either across-shore or alongshore, or be respired in sediments or the water column. Our production estimates suggest that the August POC would be, on average, over 100 mmol m^{-3} greater than in May if not respired or exported. If the POC is respired on the shelf, we expect that the average O_2 concentration would be over 150 mmol m^{-3} less in August than in May, nearly enough to deplete the entire water column of O_2. As such respiration would probably be concentrated in already-low-O_2 waters, wide-spread anoxia would result.

[40] Our observations show that the high POC levels have mostly disappeared at the seaward edge of the shelf, and this allows for only a very small fraction of the newly produced POC to escape from the system via cross-shelf Ekman transport. Standing stocks do not change significantly with time. Only about a quarter of the POC can be exported by alongshore transport. No deleterious effects of hypoxia were reported in 2001 [*Grantham et al.*, 2004]. We must therefore conclude that the above simplistic scenario is not a good description of the system.

[41] While the Oregon coastal ocean is undeniably an upwelling-dominated system during the summer months, the upwelling forcing is far from constant. Typically, several days of upwelling favorable conditions are punctuated by brief periods of reduced equator-ward, or even poleward, winds. During these "relaxation" or "reversal" periods, schematically depicted in Figure 8b, low-density offshore surface water rushes toward the shoreline, and the dense upwelled water slumps back offshore toward the shelf break through the BBL. If the BBL POC moves with the water mass, it could conceivably reach the shelf break where these isopycnals detach from the bottom. At that point, the POC can either spread along those isopycnal surfaces into the ocean interior, or sink to greater depths. We feel that the latter is far more likely. The bottom boundary layer is a likely place of coincidence of fine-grained suspended mineral material and POC. The importance of mineral ballast material in setting the settling rates of POC in the open ocean has recently been confirmed [*Armstrong et al.*, 2002; *Klaas and Archer*, 2002], and it is likely that there has been some ballasting in this setting. When this ballasted POC

reaches the shelf break, without a lower boundary to prevent further settling, it would sink rapidly to the deep ocean, far below the depths of seasonally upwelled density horizons.

[42] Some qualitative support for this hypothesis can be garnered from examination of the sections at the Cascade Head site where the bathymetry is simpler. During relaxation days (e.g., 24 May and 11 August; auxiliary material Figures S1a and S3), there is clear separation between a high-POC region in the BBL at the inshore-most extents of the section, and a second, high-POC BBL region near the shelf break. This suggests that POC has been transported seaward along with the dense, near-bottom water during relaxations, where it could potentially sink to much greater depths.

[43] Direct evidence to support this mechanism is likely to be elusive. Export should occur exclusively at the deep, offshore edges of our sections. If the POC is ballasted, and has very high sinking rates, large fluxes could be supported by relatively small concentrations which could be hard to observe. This is further complicated by the fact that the Cape Perpetua section has fairly complex bathymetry and the exact location where the onshore/offshore upwelling/relaxation cross-shelf transport occurs is uncertain. Sediment accumulation in the deep water adjacent to the shelf is in fact very high, as high as 100s of cm kyr^{-1} (A. Mix, personal communication, 2005), and carbon burial is high as well. Uncertainty over the extent of remineralization, and the area over which shelf sediments might be expected to accumulate, mean that finding a proportionate sediment deposition would be unlikely.

[44] Could this mechanism account for the residual loss of POC quantified above? We have no direct observations to quantify this, but will make a rough estimate assuming that the POC in the bottom layer is ''removed'' once every 5 days, roughly the frequency of relaxation events. If the high-POC bottom layer is 20 m thick, and contains 15 mmol m^{-3} POC (both estimates consistent with observed POC distributions), then emptying this layer into the deep ocean once every 5 days removes about 0.65 mmol m^{-3} d^{-1} of carbon from the system, about 70% of the estimated residual loss term. This estimate is of the same order of magnitude as the calculated removal flux.

[45] If such a mechanism is important for removing POC from the near-bottom waters of the shelf, then its absence might lead to long-term retention of POC in those waters, and increased likelihood that that material is respired, consuming O_2 in waters that already hover near the hypoxic threshold. While the anomalous presence of low-O_2 subarctic water at the shelf break in 2002 certainly has some bearing on the development of severe hypoxia as proposed by *Grantham et al.* [2004], another anomalous feature of the summer 2002 season was the unusually long periods of uninterrupted equatorward winds that coincided with the most significant harmful ecological effects of that summer's hypoxia event. The lack of a strong relaxation event in the 40-day period following 25 July 2002, in marked contrast to the preceding 40-day period [*Grantham et al.*, 2004] is remarkable. Persistence of the upwelling conditions depicted schematically in Figure 8b is similar to those experienced in mid-late summer of 2002, and they may well have led to the nutrient- and particle-trapping scenario discussed above, and allowed much more of the POC to be respired on the shelf, exacerbating low-O_2 conditions.

5. Conclusions

[46] Highly resolved, spatially extensive measurements spanning the upwelling season off the Oregon coast allowed quantification of the season-long rate of net production of O_2 and POC. Nearly all of the net production of organic carbon appears to be exported from the shelf, most likely to the adjacent deep ocean. This carbon export represents a long-term sequestration of atmospheric and upper thermocline carbon dioxide. If the carbon were not exported from the system, either unrealistic standing stocks of POC, or widespread anoxic near-bottom conditions would result. Some of this export is due to alongshore flow sweeping material off the downstream edge of submarine bank complexes. We speculate on an additional mechanism where POC sinks to the turbulent BBL, and aggregates and incorporates mineral ballast material while in suspension. When intermittent relaxation or reversal events interrupt prevailing upwelling conditions, this material moves to the shelf break, where it sinks with high velocities below seasonally upwelled density horizons.

[47] **Acknowledgments.** The authors are grateful to the captain and crew of the RV *Thomas G. Thompson* for their exceptional performance in executing the cross-shelf surveying operation. The assistance of L. Bandstra, P. Covert, and J. Jennings in the operation of the SuperSucker and continuous sampling and analysis systems was essential for the success of this work. Wei-Jun Cai and an anonymous reviewer made significant, constructive comments that greatly improved the originally submitted manuscript. Emmanuel Boss provided valuable comments and context for the budget calculations. Thanks are owed to J. Allen and J. Barth for leading the greater COAST program. This work was supported by NSF grant 9907854-OCE.

References

Anderson, L. A., and J. L. Sarmiento (1994), Redfield ratios of remineralization determined by nutrient data analysis, *Global Biogeochem. Cycles*, *8*, 65–80.

Armstrong, R. A., C. Lee, J. I. Hedges, S. Honjo, and S. G. Wakeham (2002), A new mechanistic model for organic carbon fluxes in the deep ocean based on the quantitative association of POC with ballast minerals, *Deep Sea Res., Part II*, *49*, 219–236.

Barth, J. A., and P. A. Wheeler (2005), Introduction to special section: Coastal Advances in Shelf Transport, *J. Geophys. Res.*, *110*, C10S01, doi:10.1029/2005JC003124.

Bender, M., J. Martin, H. Ducklow, J. Kiddon, and J. Marra (1992), The carbon balance during the 1989 spring bloom in the North Atlantic Ocean, 47°N, 20°W, *Deep Sea Res.*, *39*, 1707–1725.

Bianchi, A., L. Bianucci, A. Piola, D. Ruiz-Pino, I. Schloss, A. Poisson, and C. Balestrini (2005), Vertical stratification and air-sea CO_2 fluxes in the Patagonian shelf, *J. Geophys. Res.*, *110*, C07003, doi:10.1029/2004JC002488.

Cai, W.-J., Z. Wang, and Y. Wang (2003), The role of marsh-dominated heterotrophic continental margins in transport of CO_2 between the atmosphere, the land-sea interface and the ocean, *Geophys. Res. Lett.*, *30*(16), 1849, doi:10.1029/2003GL017633.

Castelao, R. M., and J. A. Barth (2005), Coastal ocean response to summer upwelling favorable winds in a region of alongshore bottom topography variations off Oregon, *J. Geophys. Res.*, *110*, C10S04, doi:10.1029/2004JC002409.

Chavez, F. P., and J. R. Toggweiler (1995), Physical estimates of global new production: The upwelling contribution, in *Upwelling in the Ocean: Modern Processes and Ancient Records*, edited by C. P. Summerhayes et al., pp. 313–320, John Wiley, Hoboken, N. J.

Chen, C.-T. A., A. Andreev, K.-R. Kim, and M. Yamamoto (2004), Roles of continental shelves and marginal seas in the biogeochemical cycles of the North Pacific Ocean, *J. Oceanogr.*, *60*, 17–44.

Dickson, M.-L., and P. A. Wheeler (1995), Nitrate uptake rates in a coastal upwelling regime: A comparison of PN-specific, absolute, and Chl *a*-specific rates, *Limnol. Oceanogr.*, *40*, 533–543.

Eisner, L. B., and T. J. Cowles (2005), Spatial variations in phytoplankton pigment ratios, optical properties, and environmental gradients in Oregon coast surface waters, *J. Geophys. Res.*, *110*, C10S07, doi:10.1029/2004JC002692.

Emerson, S., P. D. Quay, C. Stump, D. Wilbur, and M. Knox (1991), O_2, Ar, N_2, and ^{222}Rn in surface waters of the subarctic ocean: Net biological O_2 production, *Global Biogeochem. Cycles*, *5*, 49–69.

Emerson, S., P. D. Quay, C. Stump, D. Wilbur, and R. Schudlich (1995), Chemical tracers of productivity and respiration in the subtropical Pacific Ocean, *J. Geophys. Res.*, *100*, 15,873–15,887.

Emerson, S., P. D. Quay, D. Karl, C. Winn, L. Tupas, and M. Landry (1997), Experimental determination of the organic carbon flux from open-ocean surface waters, *Nature*, *389*, 951–954.

Garcia, H. E., and L. I. Gordon (1992), Oxygen solubility in seawater: Better fitting equations, *Limnol. Oceanogr.*, *34*, 1261–1291.

Gill, A. E. (1982), *Atmosphere-Ocean Dynamics*, 662 pp., Elsevier, New York.

Glenn, S., et al. (2004), Biogeochemical impact of summertime coastal upwelling on the New Jersey Shelf, *J. Geophys. Res.*, *109*, C12S02, doi:10.1029/2003JC002265.

Grantham, B. A., F. Chan, K. J. Nielsen, D. S. Fox, J. A. Barth, A. Huyer, J. Lubchenco, and B. A. Menge (2004), Upwelling-driven nearshore hypoxia signals ecosystem and oceanographic changes in the northeast Pacific, *Nature*, *429*, 749–754.

Hales, B., T. Takahashi, and L. Bandstra (2005a), Atmospheric CO_2 uptake by a coastal upwelling system, *Global Biogeochem. Cycles*, *19*, GB1009, doi:10.1029/2004GB002295.

Hales, B., J. N. Moum, P. Covert, and A. Perlin (2005b), Irreversible nitrate fluxes due to turbulent mixing in a coastal upwelling system, *J. Geophys. Res.*, *110*, C10S11, doi:10.1029/2004JC002685.

Harrison, W. G., T. Platt, and M. R. Lewis (1987), *f*-ratio and its relationship to ambient nitrate concentration in coastal waters, *J. Plankton Res.*, *96*, 235–248.

Hartnett, H. E., and A. Devol (2003), Role of a strong oxygen-deficient zone in the preservation and degradation of organic matter: A carbon budget for the continental margins of northwest Mexico and Washington State, *Geochim. Cosmochim. Acta*, *67*, 247–264.

Hedges, J. I., C. Lee, M. L. Peterson, S. G. Wakeham, J. A. Baldock, and Y. Gélinas (2002), The biochemical and elemental compositions of marine plankton: A NMR perspective, *Mar. Chem.*, *78*, 47–63.

Hill, J. K., and P. A. Wheeler (2001), Organic carbon and nitrogen in the northern California current system: Comparison of offshore, river plume and coastally upwelled water, *Prog. Oceanogr.*, *53*, 369–387.

Huyer, A. (2003), Preface to special section on enhanced subarctic influence in the California Current, 2002, *Geophys. Res. Lett.*, *30*(15), 8019, doi:10.1029/2003GL017724.

Karp-Boss, L., P. A. Wheeler, B. Hales, and P. Covert (2004), Distributions and variability of particulate organic matter in a coastal upwelling system, *J. Geophys. Res.*, *109*, C09010, doi:10.1029/2003JC002184.

Klaas, C., and D. Archer (2002), Association of sinking organic mater with various types of mineral ballast in the deep sea: Implications for the rain ratio, *Global Biogeochem. Cycles*, *16*(4), 1116, doi:10.1029/2001GB001765.

Kokkinakis, S. A., and P. A. Wheeler (1987), Nitrogen uptake and phytoplankton growth in coastal upwelling regions, *Limnol. Oceanogr.*, *32*, 822–829.

Kosro, P. M. (2005), On the spatial structure of coastal circulation off Newport, Oregon, during spring and summer 2001, in a region of varying shelf width, *J. Geophys. Res.*, *110*, C10S06, doi:10.1029/2004JC002769.

Kundu, P. K., and J. S. Allen (1976), Some three-dimensional characteristics of low-frequency current fluctuations near the Oregon coast, *J. Phys. Oceanogr.*, *6*, 181–199.

Lentz, S. J. (1992), The surface boundary layer in coastal upwelling regions, *J. Phys. Oceanogr.*, *22*, 1517–1539.

McGillis, W. R., J. B. Edson, J. D. Ware, J. W. H. Dacey, J. E. Hare, C. W. Fairall, and R. Wanninkhof (2001), Carbon dioxide flux techniques performed during GasEx-98, *Mar. Chem.*, *75*, 267–280.

Moum, J. N., A. Perlin, J. M. Klymak, M. D. Levine, T. Boyd, and P. M. Kosro (2005), Convectively-driven mixing in the bottom boundary layer, *J. Phys. Oceanogr.*, *34*, 2189–2202.

Muller-Karger, F. E., R. Varela, R. Thunell, R. Luerssen, C. Hu, and J. J. Walsh (2005), The importance of continental margins in the global carbon cycle, *Geophys. Res. Lett.*, *32*, L01602, doi:10.1029/2004GL021346.

Neuer, S., and T. J. Cowles (1994), Protist herbivory in the Oregon upwelling system, *Mar. Ecol. Prog. Ser.*, *113*, 147–163.

Pak, H., and J. R. Zaneveld (1977), Bottom nephloid layers and bottom mixed layers observed on the continental shelf off Oregon, *J. Geophys. Res.*, *82*, 3921–3931.

Perlin, N., R. M. Samelson, and D. B. Chelton (2004), Scatterometer and model wind and wind stress in the Oregon-California coastal zone, *Mon. Weather Rev.*, *132*, 2110–2129.

Perlin, A., J. N. Moum, and J. M. Klymak (2005a), Response of the bottom boundary layer over a sloping shelf to variations in alongshore wind, *J. Geophys. Res.*, *110*, C10S09, doi:10.1029/2004JC002500.

Perlin, A., J. N. Moum, J. M. Klymak, M. D. Levine, T. Boyd, and P. M. Kosro (2005b), A modified law-of-the-wall applied to oceanic bottom boundary layers, *J. Geophys. Res.*, *110*, C10S10, doi:10.1029/2004JC002310.

Perry, M. J., J. P. Bolger, and D. C. English (1989), Primary production in Washington coastal waters, in *Coastal Oceanography of Washington and Oregon*, pp. 117–138, edited by M. R. Landry and B. M. Hickey, Elsevier Sci., New York.

Rabalais, N. N., R. E. Turner, and W. J. Wiseman (2002), Gulf of Mexico hypoxia, a.k.a. "The Dead Zone," *Annu. Rev. Ecol. Syst.*, *33*, 235–263.

Redfield, A. C., B. H. Ketchum, and F. A. Richards (1963), The influence of organisms on the composition of seawater, in *The Sea: Ideas and Observations on Progress in the in the Study of the Seas*, vol. 2, edited by M. N. Hill, pp. 26–77, John Wiley, Hoboken, N. J.

Richardson, K., and B. B. Jorgensen (1996), Carbon flow in the water column case study: The southern Kattegat, in *Eutrophication in Coastal Marine Ecosystems*, *Coastal Estuarine Stud.*, vol. 52, edited by K. Richardson and B. B. Jorgensen, pp. 95–114, AGU, Washington, D. C.

Ruttenberg, K., and S. T. Dhyrmann (2005), Temporal and spatial variability of dissolved organic and inorganic phosphorus bioavailability in an upwelling-dominated coastal system, *J. Geophys. Res.*, *110*, C10S13, doi:10.1029/2004JC002837.

Service, R. J. (2004), New dead zone off Oregon coast hints at sea change in currents, *Science*, *305*, 1099.

Small, L. F., and D. W. Menzies (1981), Patterns of primary productivity and biomass in a coastal upwelling region, *Deep Sea Res.*, *28*, 123–149.

Small, L. F., H. Pak, D. M. Nelson, and C. S. Weimer (1989), Seasonal dynamics of suspended particulate matter, in *Coastal Oceanography of Washington and Oregon*, edited by M. R. Landry and B. M. Hickey, pp. 255–285, Elsevier Sci., New York.

Thomas, H., Y. Bozec, K. Elkalay, and H. J. W. de Baar (2004), Enhanced open ocean storage of CO_2 from shelf sea pumping, *Science*, *304*, 1005–1008.

Walsh, J. J. (1991), Importance of continental margins in the marine biogeochemical cycling of carbon and nitrogen, *Nature*, *350*, 53–55.

Walsh, J. J., P. E. Biscaye, and G. T. Csanady (1988), The 1983–1984 Shelf Edge Exchange Processes (SEEP)–I experiment: Hypotheses and highlights, *Cont. Shelf Res.*, *8*, 435–456.

Walsh, J. J., D. A. Dieterle, and J. R. Pribble (1991), Organic debris on the continental margins: A simulation analysis of source and fate, *Deep Sea Res.*, *38*, 805–828.

Wanninkhof, R. (1992), Relationship between wind speed and gas exchange over the ocean, *J. Geophys. Res.*, *97*, 7373–7382.

Zaneveld, J. R. V. (1973), Variation of optical seawater properties with depth, in *Optics of the Sea*, *AGARD Lect. Ser.*, vol. 61, pp. 2.3-1–2.3-22, North Atlantic Treaty Org., Neuilly-sur-Seine, France.

Zaneveld, J. R. V., and H. Pak (1979), Optical and particulate properties at oceanic fronts, *J. Geophys. Res.*, *84*, 7781–7790.

B. Hales, A. Perlin, and P. A. Wheeler, College of Oceanic and Atmospheric Sciences, Oregon State University, 104 Ocean Administration Building, Corvallis, OR 97331, USA. (bhales@coas.oregonstate.edu; aperlin@coas.oregonstate.edu; pwheeler@coas.oregonstate.edu)

L. Karp-Boss, School of Marine Sciences, University of Maine, 345 Aubert Hall, Orono, ME 04469, USA. (lee.karp-boss@maine.edu)